H_2 Production

DOI: 10.1002/ange.201408493

Hydrogenated Anatase: Strong Photocatalytic Dihydrogen Evolution without the Use of a Co-Catalyst**

*Ning Liu, Christopher Schneider, Detlef Freitag, Umamaheswari Venkatesan, V. R. Reddy Marthala, Martin Hartmann, Benjamin Winter, Erdmann Spiecker, Andres Osvet, Eva M. Zolnhofer, Karsten Meyer, Tomohiko Nakajima, Xuemei Zhou, and Patrik Schmuki**

Abstract: *The high-pressure hydrogenation of commercially available anatase or anatase/rutile TiO_2 powder can create a photocatalyst for H_2 evolution that is highly effective and stable without the need for any additional co-catalyst. This activation effect cannot be observed for rutile; however, for anatase/rutile mixtures, a strong synergistic effect can be found (similar to results commonly observed for noble-metal-decorated TiO_2). EPR and PL measurements indicated the intrinsic co-catalytic activation of anatase TiO_2 to be due to specific defect centers formed during hydrogenation. These active centers can be observed specifically for high-pressure hydrogenation; other common reduction treatments do not result in this effect.*

Ever since the groundbreaking research of Fujishima and Honda in 1972,[1] TiO_2 is considered a promising photocatalyst for the splitting of water into H_2 and O_2. In their original experiment, Fujishima et al. used a TiO_2 photoanode connected through an external circuit to a platinum counter-electrode; the latter was needed to successfully evolve H_2 (the fuel of the future!) from water. TiO_2, which exists in a vast variety of morphologies and modifications, has been used to initiate a wide range of photocatalytic reactions (for overviews see for example, Refs. [2–8]). While numerous photoelectrochemical studies (i.e. the use of an illuminated TiO_2 electrode in an electrochemical circuit) were performed, the most direct and economic approach is still the use of TiO_2 in the form of particle suspensions, thus employing the photocatalytic system without an externally applied voltage. However, under these so-called open-circuit conditions (OCP), TiO_2 alone is not efficient for the photoproduction of H_2 without the use of a co-catalyst (mostly, this is a noble metal (M), such as Pt, Pd, or Au; for overviews see for example, Refs. [9–11]). These combined photocatalytic M@TiO_2 systems have therefore been widely investigated in order to optimize their efficiency in the generation of H_2 from water (with or without using sacrificial agents such as ethanol).[9,12]

Anatase and rutile are the most common polymorphs in photoactivated TiO_2 applications. In photocatalytic water splitting, generally M@anatase combinations are found to be more efficient than M@rutile.[9] Nevertheless, compared to the pure phases of anatase or rutile, the presence of a mixed phase in M@TiO_2 catalysts commonly leads to a considerable enhancement of the reaction rate.[2,9]

For TiO_2-based photocatalysts, large efforts were dedicated to accelerate reaction rates and to extend the light absorption of TiO_2 (E_g anatase = 3.2 eV; E_g rutile = 3.0 eV[13]) into the visible range of the spectrum to allow a more efficient use of solar light.[2] Over the years, a large variety of band-gap engineering approaches were introduced, involving doping with a wide range of elements (for an overview, see for example, Refs. [2,8]). While the introduction of a number of extrinsic dopant states in the TiO_2 band-gap creates a visible-light activation, the effect on water-splitting efficiencies remained modest for a long time.

However, in 2011, Chen and Mao reported "black" TiO_2 particles that, when decorated with Pt, reached a very high open-circuit water-splitting activity, ascribed to a broad visible-light absorption of these "black" TiO_2.[12] This finding formed the basis for a considerable amount of follow-up work

[*] Dr. N. Liu, C. Schneider, X. Zhou, Prof.Dr. P. Schmuki
Department of Materials Science WW-4, LKO
University of Erlangen-Nuremberg
Martensstrasse 7, 91058 Erlangen (Germany)
E-mail: schmuki@ww.uni-erlangen.de

Dr. D. Freitag
High Pressure Laboratory, Chair of Separation Science and Technology, University of Erlangen-Nuremberg
Haberstrasse 11, 91058 Erlangen (Germany)

Dr. U. Venkatesan, Dr. V. R. R. Marthala, Prof.Dr. M. Hartmann
ECRC – Erlangen Catalysis Resource Center
University of Erlangen-Nuremberg
Egerlandstrasse 3, 91058 Erlangen (Germany)

B. Winter, Prof.Dr. E. Spiecker
Center for Nanoanalysis and Electron Microscopy (CENEM)
University of Erlangen-Nuremberg
Cauerstrasse 6, 91058 Erlangen (Germany)

Dr. A. Osvet
Department of Materials Sciences 6, iMEET
University of Erlangen-Nuremberg
Martensstrasse 7, 91058 Erlangen (Germany)

E. M. Zolnhofer, Prof.Dr. K. Meyer
Inorganic & General Chemistry
University of Erlangen-Nuremberg
Egerlandstrasse 1, 91058 Erlangen (Germany)

Dr. T. Nakajima
National Institute of Advanced Industrial Science and Technology
Tsukuba Central 5, 1-1-1 Higashi, Tsukuba, Ibaraki 305-8565 (Japan)

[**] We would like to acknowledge the ERC, the DFG, and the Erlangen DFG cluster of excellence (EAM) for financial support, and U. Gesenhues (Sachtleben Gmbh) for valuable discussion and providing samples. B.W. gratefully acknowledges the Research Training Group "Disperse Systems for Electronic Applications" (GRK 1161).

Supporting information for this article is available on the WWW under http://dx.doi.org/10.1002/anie.201408493.

and seemingly identical "black" TiO_2 has meanwhile been produced through a full range of conventional TiO_2-reduction treatments (vacuum annealing, electrochemical reduction, Ar/H_2 annealing under atmospheric conditions),[14–18] as well as the original H_2 treatment introduced by Chen and Mao.[12] The appearance of color in established treatments is typically ascribed to oxygen vacancies or Ti^{3+} defect states.[6,18,19] In contrast, Chen and Mao ascribed their finding to the formation of an amorphous layer at the outermost part of their TiO_2 nanoparticles.[12,20–22] Overall, for various reductive approaches, visible light absorption in TiO_2 nanoparticles and a considerable number of effects is observed, independent of the exact nature of the treatment.

Herein we show a unique co-catalytic effect that is observed specifically for TiO_2 anatase nanoparticles treated with H_2 under high pressure. Such a treatment can activate a strong and stable photocatalytic H_2 evolution in commercial anatase or anatase/rutile nanoparticles, without the use of noble-metal co-catalysts. This activation was not observed when pure rutile powders were hydrogenated. Moreover, if conventional reduction processes, for example, annealing in Ar or Ar/H_2, were used for treating the polymorphs of TiO_2, no significant activation could be found.

In our experiments, we used a range of commercially available anatase, rutile, and mixed anatase/rutile powders, as specified in the experimental section and in the Supporting Information (Table S1 and Figure S1). The typical hydrogenation was carried out in pure H_2 at 500 °C and 20 bar for durations between 1 hour and 3 days. The photocatalytic H_2-evolution activity of the different particles was evaluated by gas chromatography using suspensions of the particles in a H_2O/methanol solution under air mass coefficient (AM) 1.5 (solar simulator, Xenon lamp power supply; (100 $mW\,cm^{-2}$) illumination (experimental details are given in the Supporting Information).

Figure 1 shows the observed H_2-evolution rate of the investigated anatase, rutile, and mixed-phase samples with and without the hydrogenation treatment. After hydrogenation, clearly all anatase or anatase-containing samples show a significant photocatalytic H_2 evolution, while no H_2 generation could be detected for pure rutile samples. All untreated reference samples, anatase or rutile, did not show any detectable H_2 evolution, even for experiments carried out for up to 48 hours of illumination. Structural characterization of the particles was carried out using X-ray diffraction (XRD; Figure 2a), and on selected samples using high-resolution transmission electron microscopy (HRTEM) and selected-area electron diffraction (SAED; see the Supporting Information, Figure S2). The results show that all particles are crystalline before and after the H_2 treatment. The pure anatase samples do not show any conversion to rutile during the hydrogenation at elevated temperature (500 °C). This result is in line with reports that normally phase transition from anatase to rutile TiO_2 for nanocrystals requires annealing temperatures of more than 600 °C.[23] However, the H_2 treatment can cause the anatase content of mixed-phase particles to decrease from 12 to approximately 4% (from XRD of sample M1 in the Supporting Information, Figure S3). Both investigated mixed-phase anatase/rutile samples exhibit higher photocatalytic activity than the pure anatase samples. For sample M2, the H_2-evolution activity is more than twice the amount of that of the pure anatase sample. Some additional parameter investigations are given in the Supporting Information, Figure S4.

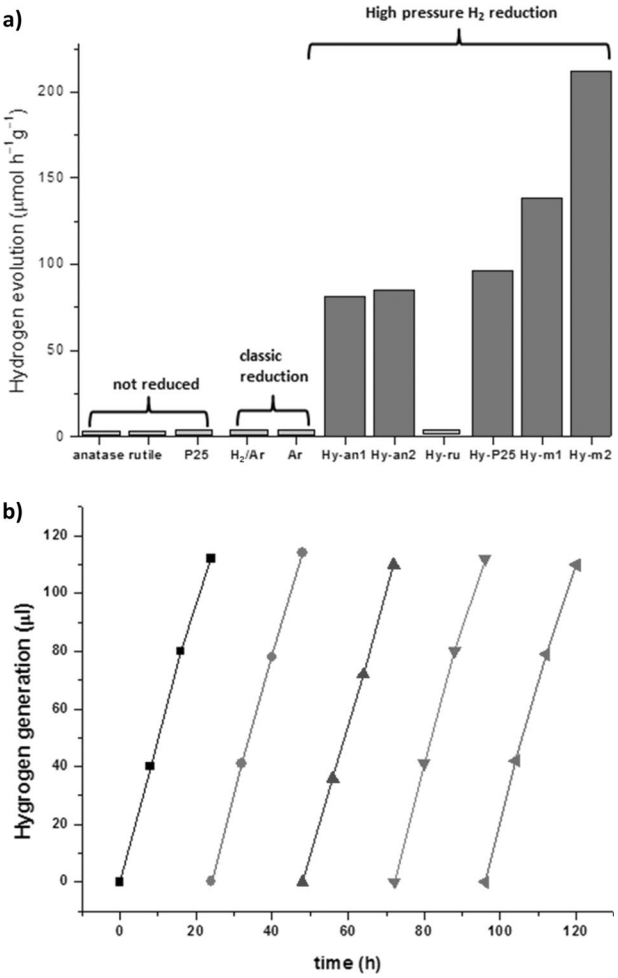

Figure 1. Rates of photocatalytic H_2 evolution from TiO_2 particle suspensions under AM 1.5 (100 $mW\,cm^{-2}$) illumination. a) Comparison of different anatase (an, an1, an2), rutile (ru), and mixed-phase (m1, m2) powders before and after hydrogenation (Hy-) at 500 °C, 20 bar (powder Ar/H_2 exposed to Ar/H_2 stream at 500 °C for 1 h; powder Ar exposed to Ar stream at 500 °C for 1 h). b) H_2 production rate from hydrogenated anatase samples (Hy-an1) over 5 days of continuous AM 1.5 illumination. P25 = TiO_2 powder (Degussa; 75% anatase, 25% rutile).

The activation is remarkably stable. Figure 1b shows H_2 evolution as a function of time over a testing period of 5 days (measured in intervals of 8 hours) using hydrogenated anatase (Hy-an1) as the photocatalyst. Over the entire investigated time, H_2 is produced at a steady rate, and there is no indication of activity-fading or poisoning.

High-temperature H_2 treatments of TiO_2 are frequently described to reduce TiO_2 in a similar manner as through the use of other reductive-gas environments, such as Ar/H_2 or high-temperature exposure to an inert gas. Therefore, except for the treatment with H_2 under high pressure, we tested Ar and Ar/H_2 treatments using anatase powder (An1 and An2).

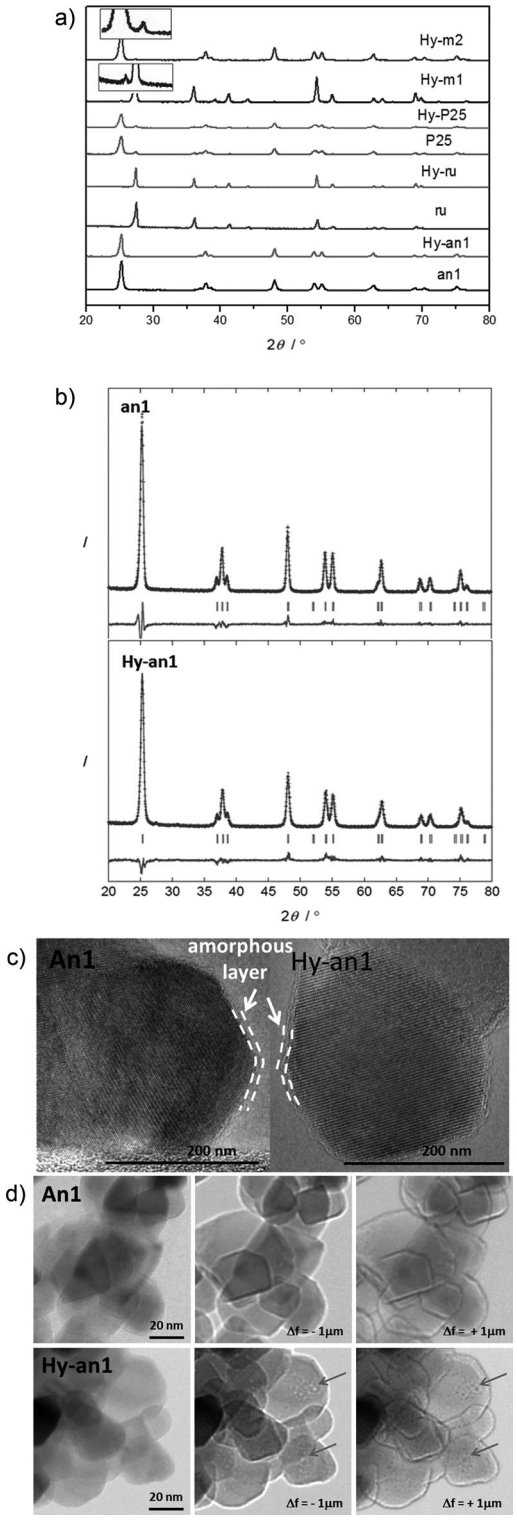

Figure 2. a) X-ray diffraction (XRD) spectra of different anatase, rutile, and mixed-phase samples used in this study. b) Rietveld refinement plot of anatase (an1) and hydrogenated anatase (Hy-an1); Lorentzian Scherrer broadening parameters: an1 $X = 0.248(6)$, Hy-an1 $X = 0.357(8)$; calculated crystallite sizes: an1 32.0 nm, Hy-an1 22.2 nm ($p = 180Kl/pX$, $K = 0.9$). c) HRTEM images of anatase before and after hydrogenation, showing no significant widening of the amorphous shell around the particle through the treatment. d) TEM bright-field images taken under focus (left), underfocus (center), and overfocus (right) conditions for anatase and hydrogenated anatase, showing characteristic Fresnel contrast, which indicates the presence of inner grain voids (arrows).

The results in Figure 1 show that for neither one of these conventional reduction treatments, a significantly stable activation for H_2 evolution could be achieved.

Reference experiments using typical noble-metal treatments on our anatase powder (Au-An1 and Pt-An1) show that at present the best measured beneficial co-catalytic effect of the H_2 treatment (Hy-an1) already achieves an efficiency of about 30% of a common Au nanoparticle co-catalyst or 10% of a common Pt treatment (see the Supporting Information, Figure S5).

In order to explore changes induced by hydrogenation and elucidate the origin of the effect, we performed further XRD, TEM, X-ray photoelectron spectroscopy (XPS), solid-state proton nuclear magnetic resonance (^{1}H MAS NMR), electron paramagnetic resonance (EPR), and photoluminescence (PL) investigations for anatase particles (An1) before and after the H_2 treatment. In order to quantify the changes from XRD of An1 before and after the treatment, we carried out a Rietveld refinement (Figure 2b and the Supporting Information, Figure S6). The results for the treated and untreated samples show a slight lattice parameter variation and clear shrinkage of the average nominal crystallite size from 32 to 22 nm. Such a reduction of the crystallite size could be due to amorphization of the original lattice induced by the H_2, if for instance, as previously observed,[12,20] the amorphous shell around the particles would increase. However, our HRTEM image of the hydrogenated particles did not show a significant increase of the thickness of these amorphous shells (Figure 2c). Nevertheless, a change induced by hydrogenation becomes apparent for TEM taken under defocus (Fresnel contrast) conditions (Figure 2d). As evident from the characteristic Fresnel contrast (bright dots in underfocus, dark dots in overfocus, see arrows), voids are present on the inside of the particles, which may explain the reduced coherent volume (seemingly reduced diameter) that is obtained from the XRD (Rietveld refinement) data. Such voids are frequently observed in anatase particles after hydrogenation, but appear also to a lesser extent in particles before treatment (see Figure S7 in the Supporting Information). The appearance of voids inside the crystalline material may be due to the internal formation of gas bubbles, as known from metals,[24] or more likely may be due to vacancy condensation.[25,26] In line with the XRD data shown in Figure 2a, the HRTEM images (Supporting Information, Figure S2) of the void-free parts of the crystal structure do not show a significant change in lattice parameters. In order to exclude beam-induced effects under HRTEM conditions (crystallization or void formation), we carried out various confirmation measurements (see for example Figure S8 in the Supporting Information).

In order to further evaluate the influence of hydrogenation, solid-state ^{1}H MAS NMR (Supporting Information, Figure S9) and XPS (Figure S10) measurements were carried out. Both methods did not give results that show a significant difference between the catalytically active and the non-active material. Nevertheless, it should be pointed out that as a result of the powder nature of the samples, ^{1}H MAS NMR

data showed strong broad peaks because of adsorbed water and OH termination,[27,28] which to a large extent originate from uptake during sample transfer to the spectrometer. Thus, it cannot be ruled out that for instance a signal from interstitial lattice H_2 is present underneath the large signal originating from adsorbed water.

However, clear changes induced by hydrogenation can be observed in EPR spectra and by PL measurements. EPR spectra taken at room temperature and at 90 K under illumination are shown in Figure 3 a. The room-temperature

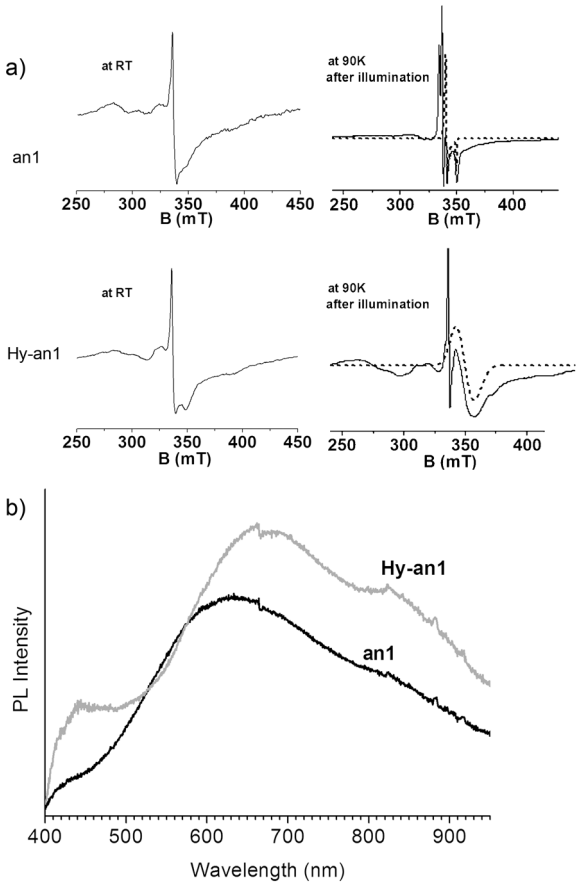

Figure 3. a) EPR spectra for anatase and hydrogenated anatase in the dark at room temperature and at 90 K after 90 min illumination. The simulations are in dotted lines: for an1 g values [1.982 1.979 1.929], g strain [0.020 0.0057 0.0068]; for Hy-an1: g values [1.960 1.905 1.905], g strain [0.070 0.090 0.080]. b) Photoluminescence of anatase and hydrogenated anatase in air using 375 nm excitation.

EPR spectrum of the nonhydrogenated anatase sample only shows a signature typically assigned to oxygen vacancies, that is, it does not indicate the presence of distinct Ti^{3+}-related signals. At 90 K, spectra taken before and after UV illumination give a clear signature with orthorhombic g values of $[g_{xx}\ g_{yy}\ g_{zz}] = [1.982\ 1.979\ 1.929]$ (obtained from the simulation of the experimental spectra using the EasySpin simulation package[29]). In contrast, the EPR spectra of the hydrogenated-anatase sample show a Ti^{3+} signature at room temperature. Furthermore, at 90 K the hydrogenated-anatase samples show a considerable increase in the Ti^{3+} signature after illumination[30] and a high intensity Ti^{3+} signal is observed after 90 min illumination with a Xe lamp (Figure 3 a). The simulation indicates an axial-symmetric Ti^{3+} ion with g values of $[g_{zz}\ g_{xx}\ g_{yy}] = [1.960\ 1.905\ 1.905]$. Other EPR features are also in line with the observed formation of H_2-evolution centers. For instance, these EPR signatures do not occur in rutile, nor are they induced by other reductive treatments (Supporting Information, Figure S11). The fact that XPS does not show the formation of surface Ti^{3+} species in substantial amounts (Supporting Information, Figure S10) indicates that they are present only in a subsurface configuration or in a concentration below the detection limit of XPS ($\approx$1 at %). Figure 3 b shows a comparison of the room-temperature PL of hydrogenated anatase (Hy-an1) with nonhydrogenated particles (An1). In both cases, a main PL peak around 600–700 nm is visible. This emission is typical for TiO_2 nanoparticles[31–33] and is a superposition of trapped-exciton and various defect-related emission bands in the anatase phase. After H_2 treatment, the overall intensity of this emission is slightly increased and its maximum is shifted to higher wavelengths. A most significant difference for the H_2-treated sample is, however, observed for the PL in the range of 400–450 nm; this peak may be related to self-trapped exciton recombination,[33–35] where excitons may be localized at neighboring Ti^{3+}-O^- sites or to band-to-localized defect transitions. Recent theoretical studies, however, shows that such neighboring sites are not stable.[36] Therefore this PL in the range just above 400 nm seems more likely associated to a sub-bandgap-defect-state to band transition. Based on the PL wavelength, defects would have to be located energetically close to the main bands, that is, at $\Delta E \approx 0.2$–0.5 eV, which is significantly closer than the $\Delta E \approx 0.8$–1.2 eV below the conduction band reported for typical Ti^{3+} states.[36,37] In this context, it is interesting that some studies on chemical vapor deposition (CVD) of suboxide layers of TiO_x ($x < 2$) found states or even a band of states very close to the anatase conduction band. These findings were supported by DFT calculations and it was reported that these states result in a higher photocatalytic activity for dye decomposition.[38]

The above experimental findings therefore clearly point toward a specific defect configuration introduced by the H_2 treatment in anatase. In theory and practice, several sub-band-gap bulk and surface electronic states have been reported to mediate the reactivity of TiO_2 in classic catalytic as well as in photocatalytic applications, and various defect configurations were reported to show a different stability in anatase and rutile structures.[6,33,36,37] Nevertheless, the findings of the present study indicate that the creation of an efficient intrinsic co-catalytic H_2-evolution activity on anatase is only achieved for treatment in pure H_2 at elevated temperature. Thus, the common assignment of features from classic reductive treatments to oxygen vacancies, Ti^{3+} states, Ti interstitials, and surface reconstruction seems not applicable in a straightforward manner.[2,6,33,36,37,39,40]

In summary, the present study demonstrates a remarkable activation of commercial anatase and anatase/rutile powders for photocatalytic H_2 evolution after hydrogenating the particles under high pressure and high temperature. The observed experimental findings on the character of the self-

induced catalytic centers resemble to a large extent the phenomenology of noble-metal co-catalytic effects on TiO_2 (such as the polymorph specificity or synergistic effects of anatase and rutile). In spite of some uncertainty about mechanistic details of this activation of anatase powders, EPR, PL, and TEM indicate that the high-pressure hydrogenation treatment supports the formation of voids in anatase nanoparticles and the formation of a specific room-temperature-stable defect structure that appears to be key for the observed co-catalytic effect on TiO_2 nanoparticles.

Received: August 24, 2014
Published online: October 19, 2014

Keywords: co-catalyst · hydrogenation · titanium(III) · TiO_2 · water splitting

[1] A. Fujishima, K. Honda, *Nature* **1972**, *238*, 37 – 38.
[2] A. Fujishima, X. Zhang, D. A. Tryk, *Surf. Sci. Rep.* **2008**, *63*, 515 – 582.
[3] A. L. Linsebigler, G. Lu, J. T. Yates, *Chem. Rev.* **1995**, *95*, 735 – 758.
[4] M. R. Hoffmann, S. T. Martin, W. Choi, D. W. Bahneman, *Chem. Rev.* **1995**, *95*, 69 – 96.
[5] A. Hagfeldt, M. Graetzel, *Chem. Rev.* **1995**, *95*, 49 – 68.
[6] U. Diebold, *Surf. Sci. Rep.* **2003**, *48*, 53 – 229.
[7] P. Roy, S. Berger, P. Schmuki, *Angew. Chem. Int. Ed.* **2011**, *50*, 2904 – 2939; *Angew. Chem.* **2011**, *123*, 2956 – 2995.
[8] I. Paramasivam, H. Jha, N. Liu, P. Schmuki, *Small* **2012**, *8*, 3073 – 3103.
[9] K. Connelly, A. K. Wahab, H. Idriss, *Mater. Renewable Sustain Energy* **2012**, *1*, 3.
[10] U. G. Akpan, B. H. Hameed, *Appl. Catal. A* **2010**, *375*, 1 – 11.
[11] M. Ni, M. K. H. Leung, D. Y. C. Leung, K. Sumathy, *Renewable Sustainable Energy Rev.* **2007**, *11*, 401 – 425.
[12] X. Chen, L. Liu, P. Y. Yu, S. S. Mao, *Science* **2011**, *331*, 746 – 750.
[13] D. O. Scanlon, C. W. Dunnill, J. Buckeridge, S. A. Shevlin, A. J. Logsdail, S. M. Woodley, C. R. A. Catlow, M. J. Powell, R. G. Palgrave, I. P. Parkin, G. W. Watson, T. W. Keal, P. Sherwood, A. Walsh, A. A. Sokol, *Nat. Mater.* **2013**, *12*, 798 – 801.
[14] A. Naldoni, M. Allieta, S. Santangelo, M. Marelli, F. Fabbri, S. Cappelli, C. L. Bianchi, R. Psaro, V. D. Santo, *J. Am. Chem. Soc.* **2012**, *134*, 7600 – 7603.
[15] G. Wang, H. Wang, Y. Ling, Y. Tang, X. Yang, R. C. Fitzmorris, C. Wang, J. Z. Zhang, Y. Li, *Nano Lett.* **2011**, *11*, 3026 – 3033.
[16] X. Lu, G. Wang, T. Zhai, M. Yu, J. Gan, Y. Tong, Y. Li, *Nano Lett.* **2012**, *12*, 1690 – 1696.
[17] S. Hoang, S. P. Berglund, N. T. Hahn, A. J. Bard, C. B. Mullins, *J. Am. Chem. Soc.* **2012**, *134*, 3659 – 3662.
[18] F. Zuo, L. Wang, T. Wu, Z. Zhang, D. Borchardt, P. Feng, *J. Am. Chem. Soc.* **2010**, *132*, 11856 – 11857.
[19] M. Anpo, M. Takeuchi, *J. Catal.* **2003**, *216*, 505 – 516.
[20] X. Chen, L. Liu, Z. Liu, M. A. Marcus, W. C. Wang, N. A. Oyler, M. E. Grass, B. Mao, P. A. Glans, P. Y. Yu, J. Guo, S. S. Mao, *Sci. Rep.* **2013**, *3*, 1510.
[21] T. Xia, C. Zhang, N. A. Oyler, X. Chen, *Adv. Mater.* **2013**, *25*, 6905 – 6910.
[22] T. Xia, W. Zhang, J. Murowchick, G. Liu, X. Chen, *Nano Lett.* **2013**, *13*, 5289 – 5296.
[23] Y. K. Kho, A. Iwase, W. Y. Teoh, L. Madler, A. Kudo, R. Amal, *J. Phys. Chem. C* **2010**, *114*, 2821 – 2829.
[24] R. Abbaschian, L. Abbaschian, R. E. Reed-Hill, *Physical Metallurgy Principies* (IV version, **2009**).
[25] J. A. Sigler and D. Kuhlmann-Wilsdorf in *The Nature of Small Defect Clusters Vol. 1* (Consultants Symp.), Ed.: M. J. Makin, Harwell Report AERE R5269, **1966**.
[26] R. M. J. Cotterill in *The Nature of Small Defect Clusters Vol. 1* (Consultants Symp.), Ed.: M. J. Makin, Harwell Report AERE R5269, **1966**.
[27] P. Jonsen, *Catal. Lett.* **1989**, *2*, 345 – 350.
[28] M. Crocker, R. H. M. Herold, A. E. Wilson, M. Mackay, C. A. Emeis, A. M. Hagedorn, *J. Chem. Soc. Faraday Trans.* **1996**, *92*, 2791 – 2798.
[29] S. Stoll, A. Schweiger, *J. Magn. Reson.* **2006**, *178*, 42 – 55.
[30] D. C. Hurum, A. G. Agrios, K. A. Gray, T. Rajh, M. C. Thurnauer, *J. Phys. Chem. B* **2003**, *107*, 4545 – 4549.
[31] C. C. Mercado, Z. Seeley, A. Bandyopadhyay, S. Bose, J. L. McHale, *ACS Appl. Mater. Interfaces* **2011**, *3*, 2281 – 2288.
[32] F. J. Knorr, J. L. McHale, *J. Phys. Chem. C* **2013**, *117*, 13654 – 13662.
[33] F. D. Angelis, C. D. Valentin, S. Fantacci, A. Vittadini, A. Selloni, *Chem. Rev.* **2014**, 114, 9708 – 9753.
[34] H. Zhang, M. Zhou, Q. Fu, B. Lei, W. Lin, H. Guo, M. Wu, Y. Lei, *Nanotechnology* **2014**, *25*, 275603.
[35] H. Yoo, M. Kim, C. Bae, S. Lee, H. Kim, T. K. Ahn, H. Shi, *J. Phys. Chem. C* **2014**, *118*, 9726 – 9732.
[36] N. A. Deskins, R. Rousseau, M. Dupuis, *J. Phys. Chem. C* **2011**, *115*, 7562 – 7572.
[37] X. Pan, M. Yang, X. Fu, N. Zhang, Y. Xu, *Nanoscale* **2013**, *5*, 3601 – 3614.
[38] I. Justicia, P. Ordejón, G. Canto, J. L. Mozos, J. Fraxedas, G. A. Battiston, R. Gerbasi, A. Figueras, *Adv. Mater.* **2002**, *14*, 1399 – 1402.
[39] Y. He, O. Dulub, H. Cheng, A. Selloni, U. Diebold, *Phys. Rev. Lett.* **2009**, *102*, 106105.
[40] P. Scheiber, M. Fidler, O. Dulub, M. Schmid, U. Diebold, W. Hou, U. Aschauer, A. Selloni, *Phys. Rev. Lett.* **2012**, *109*, 136103.

